Metasurface for Enhanced Millimeter-Wave Communications under Imperfect Beam Alignment

Jesus A. Cumana-Morales, Marceau Coupechoux, Juan Antonio Cordero Fuertes

▶ **To cite this version:**

Jesus A. Cumana-Morales, Marceau Coupechoux, Juan Antonio Cordero Fuertes. Metasurface for Enhanced Millimeter-Wave Communications under Imperfect Beam Alignment. IEEE MeditCom 2023: IEEE International Mediterranean Conference on Communications and Networking 2023, Sep 2023, Dubrovnik, Croatia. hal-04189770

HAL Id: hal-04189770

https://telecom-paris.hal.science/hal-04189770

Submitted on 29 Aug 2023

HAL is a multi-disciplinary open access archive for the deposit and dissemination of scientific research documents, whether they are published or not. The documents may come from teaching and research institutions in France or abroad, or from public or private research centers.

L'archive ouverte pluridisciplinaire **HAL**, est destinée au dépôt et à la diffusion de documents scientifiques de niveau recherche, publiés ou non, émanant des établissements d'enseignement et de recherche français ou étrangers, des laboratoires publics ou privés.

Distributed under a Creative Commons Attribution 4.0 International License

Metasurface for Enhanced Millimeter-Wave Communications under Imperfect Beam Alignment

Jesus A. Cumana-Morales*, Marceau Coupechoux†, Juan-Antonio Cordero-Fuertes‡
*Czech Technical University in Prague
†LTCI, Telecom Paris, Institut Polytechnique de Paris
‡LIX, École Polytechnique, Institut Polytechnique de Paris

***Abstract*—In this work, we investigate the impact of beam misalignment in the performance of a wireless system employing a metasurface to improve coverage in a non-line-of-sight (NLOS) scenario. The metasurface is modeled by an array of small radiating elements each of them terminated with a complex load. An equivalent Array Factor is defined, which allows visualizing the beamsteering properties of the metasurface in far-field conditions. Angular misalignment is modeled using a truncated Gaussian distribution and an expression to evaluate signal-to-noise ratio (SNR) in the presence of misalignment is derived. Numerical results show an SNR degradation close to 8 dB for 5° error magnitude and up to 14 dB if high-gain unit cells are used. Three mechanisms are explored, which can be used to reduce SNR degradation: increasing Metasurface dimensions allows recovering SNR by 7.4 dB, low unit cell gain allows improving SNR by close to 10.5 dB when compared to a high-gain cell and base station beamwidth decrease from 25.6° to 12.7° allows recovering SNR by 4 dB thanks to the higher BS beam gain.**

***Index Terms*—Metasurface, millimeter wave, misalignment, beamforming.**

I. Introduction

Metasurfaces (MS) are composed of periodic or quasi-periodic sub-wavelength unit cells arranged on a 2-D surface [1]. The exceptional electromagnetic properties of these planar metamaterials make them attractive in areas such as waveform shaping, polarization conversion, broadband absorbers and optical filters, among others [2]. In millimeter-wave (mm-Wave) wireless communications, MS have been studied as a mean of controlling the propagation environment to increase quality of service. In this respect, they are also called *large intelligent surfaces* (LIS), *reconfigurable intelligent surfaces* (RIS or IRS) or *software-controlled metasurfaces* [3].

RIS have been extensively studied in the literature. For instance, the propagation characteristics and pathloss modeling of RIS-assisted communications are presented in [4]. A RIS-enhanced OFDM system is also investigated in [5]. Those studies seem to indicate that RIS is a very promising technique for improving coverage or capacity.

Despite offering large potential benefits, RIS-based systems have some disadvantages, which make them less attractive in some applications. In [6] some of these drawbacks are listed: (1) a dedicated control channel (CC) is required for real-time RIS configuration, causing signaling overhead, additional complexity and cost, (2) RIS need to be powered, which increases energy consumption and might not be feasible in some scenarios, (3) the estimation of the channel state information (CSI) is quite challenging. Due to these factors, the use of full passive and non-reconfigurable MS as an alternative to RIS is discussed in [6]. The authors propose to use a frequency-selective MS to improve coverage of short-range OFDM wireless networks.

In [6], each data stream in the OFDM system is reflected in a desired direction by properly assigning subcarriers to users without the need of CC and dedicated CSI estimation. For this purpose, the reflection phase shift of the MS has to be properly designed. The dimensions of the metasurface play an important role in the angle selectivity of the system. Increasing the size of the MS might result in angle gaps; as a consequence, low signal-to-noise ratio (SNR) is obtained for users within those gaps. Although this issue was not further investigated by the authors in [6], they propose to increase the number of carriers or to decrease the bandwidth (BW) to compensate for this effect. In the work presented in [7], transmission through a RIS with phase errors is analyzed. The authors assume that perfect phase estimation or high-precision configuration of the RIS is not feasible and describe phase errors using a generic distribution. Although the work in [7] shows how to determine average probability of error as a function of phase estimation and quantization errors, it assumes a single-antenna source and does not address performance in a wireless communication scenario. Phase quantization errors do not play a role in a fully passive MS but alignment of the base station (BS) beam with respect to the MS might have an effect on angular gaps, and therefore on users coverage. The impact of beam alignment error (BAE) in device-to-device mm-Wave communications has been addressed by several authors, *e.g.*, [8], [9], but has not been investigated in a MS-assisted wireless systems. This paper extends the work in [6] to MS-assisted scenarios with imperfect beam alignment. The contribution of this paper can be summarized as follows:

- We propose to use a truncated Gaussian distribution to describe the angular error of the beam impinging in the MS.
- We derive an expression for the SNR experienced at a user receiving a signal from the MS in the presence of beam misalignment errors at the BS.
- Our study shows that beam misalignment causes severe

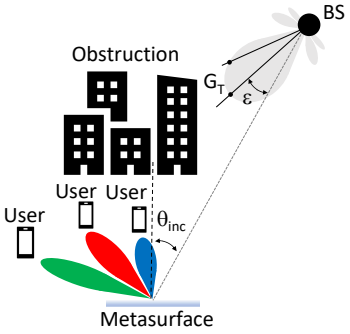

Fig. 1. BS-users NLOS transmission assisted by a metasurface.

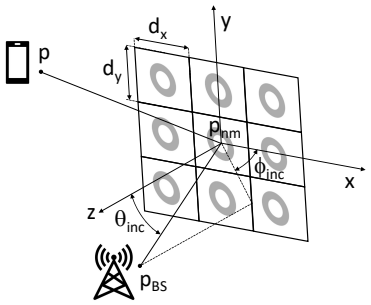

Fig. 2. Metasurface with elementary cells.

SNR degradation and proposes three mechanisms, which can help overcoming this problem, namely: increasing MS dimensions, selecting low-gain unit cells and using narrower BS beamwidth.

In the rest of this paper, we introduce a general description and simplified model of the MS in Section II. Section III presents the system model and section IV-B the coverage evaluation. Numerical results are shown in Section V. Section VI concludes the paper.

II. Metasurfaces in Wireless Systems

In the context of this paper, the MS is used to enhance coverage in a Non-Line-Of-Sight (NLOS) wireless communication between a BS and a UE (Fig. 1). The BS signal is supposed to be obstructed by surrounding buildings. The transmitter (Tx) might still reach the UE thanks to scattering, but this approach is limited to a mere specular reflection. Alternatively, a MS can be used to control the Angle of Departure (AoD) of the reflected signal, allowing to reach the desired UE.

A. General Description

The MS is depicted in Fig. 2 and is represented by a surface in the $x-y$ plane with center at $\mathbf{p}_0 = (0,0,0)$. It is composed of $N \times M$ elementary cells of size $d_x \times d_y$, distributed in a grid of points with coordinates $\mathbf{p}_{nm} = (x_n, y_m, 0)$. For simplicity, we assume a MS with an odd number of unit cells, therefore $x_n = n \cdot d_x$ and $y_m = m \cdot d_y$ with $|n| \leq (N-1)/2$ and $|m| \leq (M-1)/2$. The surface size is $L_x \times L_y$ with $L_x = N \cdot d_x$ and $L_y = M \cdot d_y$. The dimensions d_x and d_y of each unit cell along the x and y axis respectively, are usually in the sub-wavelength range of $\left[\frac{\lambda}{10}, \frac{\lambda}{2}\right]$ [10]. A BS located at point $\mathbf{p}_{\text{BS}}$ transmits a signal, which impinges the MS with an angle $\Theta_{\text{inc}} = (\theta_{\text{inc}}, \phi_{\text{inc}})$. The UE is located at point $\mathbf{p}$ and receives the reflected signal at the observation angle $\Theta = (\theta, \phi)$.

B. Simplified Model

Each unit cell of the MS can be represented by an antenna element terminated with a cell-dependent and frequency-dependent load impedance $Z_{nm}(f)$ [6]. The reflection coefficient for an incident plane wave impinging at angle $\Theta_{\text{inc}} = (\theta_{\text{inc}}, \phi_{\text{inc}})$ and observed at $\Theta = (\theta, \phi)$ is given by [6], [10]:

$$\begin{aligned} r_{nm}(\widehat{\Theta}_{\text{inc}}, \Theta_{\text{inc}}, \Theta, f) &= \Gamma_{nm}(f) \cdot \\ &\quad \sqrt{P^{\text{BS}}(\widehat{\Theta}_{\text{inc}})\, P(\Theta_{\text{inc}})\, P(\Theta)\, G_c} \\ &= \beta_{nm}(\widehat{\Theta}_{\text{inc}}, \Theta_{\text{inc}}, \Theta, f) \cdot e^{j\Psi_{nm}(f)} \end{aligned} \tag{1}$$

where $P^{\text{BS}}(\Theta)$ and $P(\Theta)$ are the normalized power radiation pattern (PRP) of the BS and of the unit cell respectively, which are assumed to be frequency-independent within the BW of interest. The unit cell gain is denoted by $G_c = 4\pi(d_x\, d_y)/\lambda^2$ and $\Gamma_{nm}(f)$ represents the frequency-dependent load reflection coefficient. Variables β_{nm} and Ψ_{nm} represent the magnitude and phase of the unit cell reflection coefficient respectively.

The factor $P^{\text{BS}}(\widehat{\Theta}_{\text{inc}})$ quantifies the misalignment between the BS beam and the MS with $\widehat{\Theta}_{\text{inc}} = (\varepsilon, \widehat{\phi}_{\text{inc}})$ being the deviation of the PRP maximum from the ideal position indicated by the dotted line in Fig. 1. Note that when there is no misalignment (i.e., the BS beam is pointing to the MS center), we have $\widehat{\Theta}_{\text{inc}} = (0,0)$ and thus $P^{\text{BS}}(0,0) = 1$. An example of normalized PRP is shown in (2):

$$P(\Theta) = \begin{cases} \cos^q(\theta) & \theta \in [0, \pi/2], \phi \in [0, 2\pi], \\ 0 & \text{otherwise.} \end{cases} \tag{2}$$

Two values are proposed in the literature, namely, $q = 3$ [10] and $q = 0.57$ [11].

The load reflection coefficient in (1) is given by:

$$\Gamma_{nm}(f) = \frac{Z_{nm}(f) - Z_0}{Z_{nm}(f) + Z_0}, \tag{3}$$

where Z_0 is the reference antenna impedance. The reflection characteristics of the MS can be modified by an appropriate design of the load impedance $Z_{nm}(f)$. The phase $\Psi_{nm}(f)$ can for example be designed to be linear with the frequency [6]:

$$\Psi_{nm}(f) = \alpha_{nm} \cdot (f - f_r) \tag{4}$$

where α_{nm} is a cell-dependent coefficient and f_r a reference frequency, which could be set to f_0 (center frequency) or to $f_0 - W/2$ (lowest edge of the band) (W is the signal BW).

III. System Model

The space surrounding an antenna is usually subdivided in three regions: reactive near-field, radiating near-field (Fresnel), and far-field (Fraunhofer) regions [12]. The last two regions are defined in terms of the radii d_{Fresnel} and $d_{\mathrm{Fraunhofer}}$[1]. We consider here an outdoor scenario[2] and assumes the Tx to receiver (Rx) separation to be large enough for the far-field case to hold (i.e., $d \geq d_{\mathrm{Fraunhofer}}$). As an example, for $f_0 = 28$ GHz, $d_{\mathrm{Fraunhofer}} = 47$ m for a MS with a maximum side length of 50 cm.

A. Channel Model

The wireless system under consideration is operating in NLOS conditions but it is assumed that both the BS and the UE are in LOS with respect to the MS. As shown in Fig. 2, the BS is located at position $\mathbf{p}_{\mathrm{BS}}$ and the Rx at position $\mathbf{p}$. In order to determine the received signal at $\mathbf{p}$, two complex channel gain equations can be set, one for the BS-MS path and the other for the MS-UE path. The previously defined complex reflection coefficient of the MS is included in the total complex gain response. As a consequence, the received signal at the UE on the k-th subcarrier can be written as:

$$y^{(k)} = \sqrt{P_T} \cdot c^{(k)}(\mathbf{p_{BS}}, \mathbf{p}) \cdot \omega^{(k)} \cdot x^{(k)} + n^{(k)} \qquad (5)$$

where $x^{(k)} \in \mathbb{C}$ represents the transmitted signal (or symbol), P_T the total transmitted power and $\omega^{(k)} \in \mathbb{R}^+$ denotes the weights for power allocation among subcarriers and fulfill $\sum_k \left(\omega^{(k)}\right)^2 = 1$. The cascaded channel coefficient $c^{(k)}(\mathbf{p_{BS}}, \mathbf{p})$ for the far-field case is given by:

$$\begin{aligned} c^{(k)}(\mathbf{p_{BS}}, \mathbf{p}) &= h_0 \cdot g_0 \cdot \beta_0^{(k)}(\Theta_{\mathrm{inc}}, \Theta) \\ &\quad \cdot \sum_{n=0}^{N-1} \sum_{m=0}^{M-1} \exp\Big(\jmath \cdot \kappa \cdot n \cdot d_x \cdot U_x^+(\Theta_{\mathrm{inc}}, \Theta) \\ &\quad + \jmath \cdot \kappa \cdot m \cdot d_y \cdot U_y^+(\Theta_{\mathrm{inc}}, \Theta) + \jmath\, \Psi_{nm}^{(k)}\Big) \qquad (6) \end{aligned}$$

where h_0 and g_0 account for the free-space loss and are defined as follows:

$$h_0 = \frac{\lambda\sqrt{G_{\mathrm{T}}}}{4\pi|\mathbf{p_{BS}}|} e^{-j\,\kappa|\mathbf{p_{BS}}|} \qquad (7)$$

$$g_0 = \frac{\lambda\sqrt{G_{\mathrm{R}}}}{4\pi|\mathbf{p}|} e^{-j\,\kappa|\mathbf{p}|} \qquad (8)$$

In (7) and (8), G_{T} and G_{R} are the Tx and Rx antenna gains respectively and $\kappa = 2\pi/\lambda$. Note that in (6) we have omitted the dependency on $\widehat{\Theta}_{inc}$ to simplify the notation. Furthermore, the frequency dependency[3] of the MS reflection coefficient is now denoted as a subcarrier dependency, i.e., $\beta_0^{(k)}(\Theta_{\mathrm{inc}}, \Theta) = \beta_0(\Theta_{\mathrm{inc}}, \Theta, f_k)$ and $\Psi_{nm}^{(k)} = \Psi_{nm}(f_k)$. In addition to this, due to the far-field approximation[4] only the phase component of $c^{(k)}(\mathbf{p}_{\mathrm{BS}}, \mathbf{p})$ is a function of the cell location $(n\,d_x, m\,d_y)$.

The following quantities are defined for convenience:

$$U_x^{\pm}(\Theta_{\mathrm{A}}, \Theta_{\mathrm{B}}) = \sin(\theta_{\mathrm{A}})\cos(\phi_{\mathrm{A}}) \pm \sin(\theta_{\mathrm{B}})\cos(\phi_{\mathrm{B}}) \qquad (9)$$

$$U_y^{\pm}(\Theta_{\mathrm{A}}, \Theta_{\mathrm{B}}) = \sin(\theta_{\mathrm{A}})\sin(\phi_{\mathrm{A}}) \pm \sin(\theta_{\mathrm{B}})\sin(\phi_{\mathrm{B}}) \qquad (10)$$

where $\Theta_{\mathrm{inc}} = (\theta_{\mathrm{inc}}, \phi_{\mathrm{inc}})$ is the incident or Angle-of-Arrival (AoA) at the MS, and $\Theta = (\theta, \phi)$ is the observation angle or AoD at the MS towards the UE.

B. Beamsteering

The signal impinging on the MS needs to be deflected towards a target direction $\Theta_0^{(k)} = \left(\theta_0^{(k)}, \phi_0^{(k)}\right)$ according to a pre-selected carrier frequency f_k. To accomplish this, the phase $\Psi_{nm}^{(k)}$ of the MS reflection coefficient has to fulfill:

$$\Psi_{nm}^{(k)} = -\kappa \cdot n \cdot d_x \cdot U_x^+(\Theta_{\mathrm{inc}}, \Theta_0^{(k)}) - \kappa \cdot m \cdot d_y \cdot U_y^+(\Theta_{\mathrm{inc}}, \Theta_0^{(k)}) \qquad (11)$$

Replacing (11) in (6), we obtain:

$$\begin{aligned} c^{(k)}(\mathbf{p_{BS}}, \mathbf{p}) &= h_0 \cdot g_0 \cdot \beta_0^{(k)}(\Theta_{\mathrm{inc}}, \Theta) \\ &\quad \cdot \sum_{n=0}^{N-1} \sum_{m=0}^{M-1} \exp\Big(\jmath \cdot \kappa \cdot n \cdot d_x \cdot U_x^-(\Theta, \Theta_0^{(k)}) \\ &\quad + \jmath \cdot \kappa \cdot m \cdot d_y \cdot U_y^-(\Theta, \Theta_0^{(k)})\Big) \qquad (12) \end{aligned}$$

Equation (12) can be re-written as follows:

$$c^{(k)}(\mathbf{p_{BS}}, \mathbf{p}) = h_0 \cdot g_0 \cdot \beta_0^{(k)}(\Theta_{\mathrm{inc}}, \Theta) \cdot AF^{(k)}(\Theta) \qquad (13)$$

where $AF^{(k)}(\Theta)$ represents the equivalent array factor (AF) of the Tx-MS system and is given by[5]:

$$AF^{(k)}(\Theta) = \sum_{n=1}^{N} \exp\Big(\jmath(n-1)\widehat{\Psi}_x\Big) \sum_{m=1}^{M} \exp\Big(\jmath(m-1)\widehat{\Psi}_y\Big) \qquad (14)$$

with $\widehat{\Psi}_x = \kappa d_x U_x^-(\Theta, \Theta_0^{(k)})$ and $\widehat{\Psi}_y = \kappa d_y U_y^-(\Theta, \Theta_0^{(k)})$.

In order to be able to plot the AF, the target direction $\Theta_0^{(k)}$ needs to be related to the incident angle Θ_{inc} and to the reflection phase properties of the MS. The following expression for α_{nm} is obtained [6]:

$$\alpha_{nm} = -\left(\frac{4\pi}{\lambda W}\right)\Big[\sin(\theta_{\mathrm{inc}}) + \sin(\theta_0^{(K)})\Big] \cdot x_n \qquad (15)$$

where $W = 2(f_K - f_0)$ and $\theta_0^{(K)}$ represents the desired reflection angle at the highest subcarrier, i.e., for $k = K$. Equation (15) is obtained under the assumptions $\Theta_{\mathrm{inc}} = (\theta_{\mathrm{inc}}, 0)$ and $\Theta_0^{(K)} = (\theta_0^{(K)}, 0)$.

The simplified expression for the AF from (14) can now be written as:

$$AF^{(k)}(\Theta) = M \cdot \sum_{n=1}^{N} \exp\Big(\jmath(n-1)\kappa d_x \left(\sin(\theta) - \sin(\theta_0^{(k)})\right)\Big) \qquad (16)$$

[1] $d_{\mathrm{Fraunhofer}} = 2\,D^2/\lambda$ and $d_{\mathrm{Fresnel}} = 0.62\sqrt{D^3/\lambda}$, where D is the largest dimension of the MS [12].

[2] According to [13], outdoor cell sizes for 5G mm-Wave are on the order of 100 m to 200 m.

[3] As will be shown subsequently, Ψ_{nm} also depends on Θ, Θ_{inc}, signal BW, etc. Nevertheless, for the sake of simplification only the position (x_n, y_m) and subcarrier dependency k is indicated.

[4] $|\mathbf{p}_{\mathrm{BS}} - \mathbf{p}_{nm}| \approx |\mathbf{p}_{\mathrm{BS}} - \mathbf{p}_0| = |\mathbf{p}_{\mathrm{BS}}|$, $|\mathbf{p} - \mathbf{p}_{nm}| \approx |\mathbf{p} - \mathbf{p}_0| = |\mathbf{p}|$ and $\beta_{nm}^{(k)}(\Theta_{\mathrm{inc}}, \Theta) = \beta_0^{(k)}(\Theta_{\mathrm{inc}}, \Theta)$.

[5] The normalized array factor is $AF_{\mathrm{norm}}^{(k)}(\Theta) = \left(\frac{1}{N \cdot M}\right) AF^{(k)}(\Theta)$.

where:

$$\sin\left(\theta_0^{(k)}\right) = (a_k - 1)\cdot\sin\left(\theta_{\text{inc}}\right) + a_k \cdot \sin\left(\theta_0^{(K)}\right) \quad (17)$$

with $a_k = 2(f_k - f_0)/W$. At the center frequency specular reflection holds, i.e., $\theta_0^{(K/2)} = -\theta_{inc}$ and at the highest carrier $\theta_0^{(K)} = -\theta_{inc} - \theta_m$, where θ_m defines the desired angular range to be covered by the MS through reflection.

A numerical example is provided to visualize the AF. Following values are used: $\theta_{\text{inc}} = 30°$, $\phi_{\text{inc}} = 0$, $\theta_m = 30°$, $f_0 = 28$ GHz, $W = 10$ MHz, $N = M = 100$, $d_x = d_y = \lambda/2$ and $K = 256$. Fig. 3 shows the AF for a selected subset of 4 subcarriers (with $f_{k=130} \approx 28$ GHz), in which the main lobe shifts[6] in 5° steps starting from $-25°$ for $k = 105$ to $-40°$ for $k = 180$. A hypothetical 5°-deviation in θ_{inc}, due to e.g. BS beam resolution, would cause the AF beams to shift. A UE operating at for instance $k = 130$ would now require to operate at $k = 105$ or $k = 155$ to get a better signal from the BS. This example illustrates that BS beam misalignment might be in part addressed by User subcarrier re-assignment. The dotted curve in Fig. 3 shows that a wider beam is obtained by reducing the number of cells to $N = M = 50$. This wider beam exhibits lower gain but might be advantageous if misalignment is to be taken into account. This trade off between gain and beamwidth is studied in our numerical analysis section.

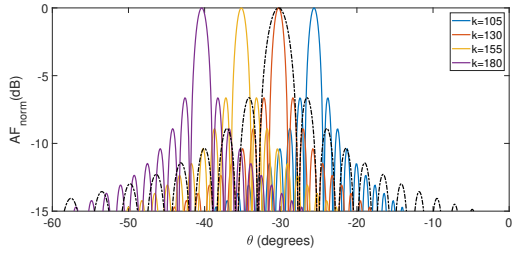

Fig. 3. Array factor for $\theta_{\text{inc}} = 30°$, $\theta_m = 30°$, $f_0 = 28$ GHz, $W = 10$ MHz and $N = M = 100$. Dotted line corresponds to $N = M = 50$.

IV. Beam Alignment Error

The directional antenna pattern can be modeled using again a cosine expression as previously done for the PRP of the MS cells (see (2)). In [8], the following normalized PRP is proposed:

$$P^{\text{BS}}(\widehat{\Theta}_{\text{inc}}) = \begin{cases} \cos^2(\frac{\tau\varepsilon}{2}) & |\varepsilon| \le \frac{\pi}{\tau}, \widehat{\phi}_{\text{inc}} \in [0, 2\pi] \\ 0 & \text{otherwise.} \end{cases} \quad (18)$$

where the parameter τ controls the width of the antenna beam. $\widehat{\Theta}_{\text{inc}}$ has an elevation and an azimuthal component but for our analysis we will assume the azimuthal error to be zero, i.e. $\widehat{\Theta}_{\text{inc}} = (\varepsilon, 0)$, where ε is an angular deviation, which in the ideal case (antenna beam pointing to MS) becomes zero. The deviation of the beam bore sight might be caused by non-perfect AoA estimation by the Rx [8] as well as due to the scanning resolution of the Tx beamformer.

[6]Total shift in this example is $\theta_0^{(1)} \approx -8°$ to $\theta_0^{(256)} = -60°$.

A. Alignment Error Distribution

In the considered scenario, the BS beam would ideally be pointing towards the center of the MS, resulting in maximum gain. Due to the beam alignment error (BAE) $\widehat{\Theta}_{\text{inc}} = (\varepsilon, 0)$, the angle of incidence deviates from the optimum case.

Following the approach in [9], we assume the angle of incidence error ε to be a random variable with probability density function (PDF) f_ε. The angle of incidence is therefore $\theta_{\text{inc}} + \varepsilon$, with ε taking values in the interval $[-\pi/(2\,\tau), \pi/(2\,\tau)]$. The mean of the Tx PRP in the direction ε is:

$$\mathbb{E}[P^{\text{BS}}(\varepsilon)] = \int_{-\pi/\tau}^{\pi/\tau} P^{\text{BS}}(x)\, f_\varepsilon(x)\, dx \quad (19)$$

The interval $[-\pi/(2\,\tau), \pi/(2\,\tau)]$ corresponds to the *Half-Power Beamwidth*[7] (HPBW). Furthermore, the PDF of ε can be expressed by using a truncated Gaussian distribution with zero mean and variance σ^2 [9] [14]:

$$f_\varepsilon(x) = \frac{1}{\sqrt{2\pi}\sigma} \frac{\exp\left(-\frac{x^2}{2\,\sigma^2}\right)}{erf\left(\frac{\pi/\tau}{\sqrt{2}\sigma}\right)}, \; |x| \le \frac{\pi}{2\,\tau} \quad (20)$$

where $erf(\cdot)$ is the Gaussian error function defined as $erf(x) = \frac{2}{\sqrt{\pi}} \int_0^x e^{-t^2}\, dt$.

The selection of the truncation limits above requires further explanation. In mm-Wave systems, beamforming (BF) can be implemented using the so-called Codebook-based BF. In this technique, the BS transmits reference signals and the UE performs channel estimations to requests specific beam directions from the BS, the UE can select among a list of predefined beam directions (precoding codebook) [15]. Codebook design is important to maximize coverage using a finite number of beams. Furthermore, codebooks with overlapping beams can be considered in order to provide robustness again BAE [16]. For the purpose of this work, we assume that the BS uses overlapping beams and for the sake of simplicity we consider that the beams intersect at the HPBW.

B. Coverage evaluation

The reflection coefficient of the MS can now be written in such a way that it accounts for beam misalignment as[8]:

$$\begin{aligned} r_{nm}(\varepsilon, \theta_{\text{inc}}, \theta, f) &= \sqrt{P^{\text{BS}}(\varepsilon)\, P(\theta_{\text{inc}} + \varepsilon)\, P(\theta)\, G_c}\, \Gamma_{nm}(f) \\ &= \beta_{nm}(\varepsilon, \theta_{\text{inc}}, \theta, f)\, e^{j\Psi_{nm}(f)} \end{aligned} \quad (21)$$

and (13) can be re-written as follows:

$$c^{(k)}(\mathbf{p_{BS}}, \mathbf{p}) = h_0\, g_0\, \beta_0^{(k)}(\varepsilon, \theta_{\text{inc}}, \theta) AF^{(k)}(\varepsilon, \theta_{\text{inc}}, \theta) \quad (22)$$

Now, let $P_T |c^{(k)}(\mathbf{p_{BS}}, \mathbf{p})\, \omega^{(k)}|^2$ be the power of the transmitted signal $x^{(k)}$ and W the signal BW, then the SNR can be expressed as follows:

$$SNR = \frac{P_T \left|c^{(k)}(\mathbf{p_{BS}}, \mathbf{p})\, \omega^{(k)}\right|^2}{N_0\, W} \quad (23)$$

[7]HPBW: angular separation between the half-power points of the main antenna beam.

[8]Note that lower case θ is used in $r_{nm}(\varepsilon, \theta_{\text{inc}}, \theta, f)$ as the PRP under consideration dependent solely on the elevation angle.

TABLE I
SIMULATION PARAMETERS

Parameter	Notation	Value
Center Frequency	f_0	28 GHz
Tx power	P_T	33 dBm
Tx antenna gain	G_{T}	27 dBi
Rx antenna gain	G_{R}	6 dBi
Rx noise figure	F	5 dB
Bandwidth	W	800 MHz
Noise Power Spectral Density	N_0	-174 dBm/Hz
Path-loss exponent	α	2

where N_0 is the power spectral density of noise. The SNR can be written as shown in (24) by using (22), (21), (18) and (2).

As indicated by (23) reducing W would allow increasing SNR (at the expense of channel capacity). On the other hand, according to (15) reducing W would result in higher values of α_{nm} (the slope of the unit cell reflection coefficient phase), which is a measure of the frequency selectivity of the MS. Creating a strong frequency selectivity requires significant change on the reactance of the cell impedance, which might be challenging to achieve over a smaller BW.

V. NUMERICAL STUDY

For our numerical experiments the values in Tab. I are used.[9] A square-shaped MS of length L is assumed and the cell is characterized by $d_x = d_y = \lambda/2$ and $N = M = \lfloor L/dx \rfloor$. A free-space path-loss model is employed. The goal here is to determine the effect of BAE on SNR. For this purpose, we perform Monte-Carlo simulations with 100k iterations. Further, we assume that the BS and the UE are both located at 100 m from the MS. In addition to this, we are considering only one subcarrier, the one with $f_k = f_0$.

Fig. 4 (left axis) shows the SNR as a function of the standard deviation of the error (σ) for four different values of the MS length L, $\theta_{\mathrm{inc}} = 30^\circ$ and $\tau = 12$. The parameter τ was calculated by assuming a HPBW $= 15^\circ$, which is a realistic value for 28 GHz arrays [18]. As can be seen in Fig. 4, the SNR strongly decays with σ, causing ≈ 8 dB degradation for $\sigma = 5^\circ$ and $L = 40$ cm. On the other hand, SNR can be recovered by 7.4 dB by increasing the MS area from 40×40 cm^2 to 70×70 cm^2. This is due to the larger number of unit cells: In this case, approximately three times more cells can be accommodated in the MS, which should result in a theoretical $20\log_{10}(3) = 9.5$ dB SNR gain. Fig. 4 (right axis) shows $\Delta\mathrm{SNR} = \mathrm{SNR}_{70cm} - \mathrm{SNR}_{40cm}$, the SNR gain obtained by increasing the size of the MS. The theoretical gain of 9.5 dB can be observed at $\sigma = 0^\circ$. However, the SNR gain ΔSNR decreases to 2.3 dB when the BAE error increases to $\sigma = 5^\circ$. This reduction can be explained by the narrower AF beam when there are more cells and the fact that a narrower beam is more sensitive to beam misalignment. Despite this SNR gain reduction at higher σ, a larger MS, with higher beam gain, results in a better SNR.

Equation (2) in Section II-B describes the PRP of the MS unit cells and two values for the parameter q were considered. Using $q = 0.57$ results in a bore-side gain of 5 dBi whereas $q = 3$ results in 9 dBi. The effect on the SNR when using these two values of q is depicted in Fig. 5 for two different incidence angle. We first observe that whatever q, increasing the incidence angle degrades the SNR. The SNR loss is however particularly important when the unit cell is more directive ($q = 3$). When going from $\theta_{\mathrm{inc}} = 30^\circ$ to 60 and at $\sigma = 0^\circ$, the loss is 14.3 dB with $q = 3$, whereas it is only 2.7 dB with $q = 0.57$. In the presence of a misalignment error of $\sigma = 5^\circ$, the losses are 11 dB and 0.5 dB respectively. As a conclusion, less directive unit cells bring a SNR improvement of about 10.5 dB at high incidence angles and are less sensitive to misalignment errors.

We now evaluate the impact of the BS beamwidth. Assume that the BS array has $N_x^{BS} \times N_y^{BS}$ elements, each of them with a 8 dBi gain. An array of 9×9 elements results for example in a beam gain of $G_{\mathrm{T}} = 27$ dBi. As we are considering misalignment in the elevation angle θ only, N_y^{BS} is varied, while N_x^{BS} is set to 9. The HPBW is a function of N_y^{BS} and can be calculated as shown in [12] (section 6.3). The value of τ to be used in (18) is equal to π/HPBW.

We have assumed so far overlapping beams as a means to provide robustness against BAE [16]. Under this assumption, the truncation limits in (20) are given by $\pm 0.5 \cdot \mathrm{HPBW}$. For comparison purposes, we also study the case of non-overlapping beams. This results in truncation limits of $\pm 0.5 \cdot \mathrm{FNBW}$, where FNBW represents the *First-Null Beamwidth* and can be approximated as $\mathrm{FNBW} \approx 2 \cdot \mathrm{HPBW}$ [12].

Fig. 6 shows the SNR vs. σ for 4 values of N_y^{BS}. The solid lines are for overlapping beams (legend with subscript HPBW) whereas the dashed lines for non-overlapping beams (subscript FNBW). The value of HPBW for each N_y^{BS} is also noted in the figure. An SNR degradation of 9.5 dB is observed with $N_y^{BS} = 10$ for $\sigma = 5^\circ$. For non-overlapping beams this number is 11 dB. The array having $N_y^{BS} = 4$ displays an SNR degradation of 11 dB at $\sigma = 5^\circ$ for the overlapping case (1.5 dB worse than for $N_y^{BS} = 10$) as well as for the non-overlapping case and therefore no advantage is observed from overlapping, which also implies that less beams are required with this array. Further, reducing the HPBW by half (25.6° to 12.7°) allows SNR improvement by 4 dB at

[9] Values taken from [17] with the exception of Rx antenna gain. We assume that the MS is able to operate over the specified BW of 800 MHz.

$$SNR = \frac{P_T \left| \left(\frac{\lambda}{4\pi}\right) \frac{\sqrt{G_{\mathrm{T}} G_{\mathrm{R}}}}{|\mathbf{p}_{\mathrm{BS}}||\mathbf{p}|} \sqrt{\cos^2\left(\frac{\tau}{2}\varepsilon\right) \cos^q(\theta_{\mathrm{inc}} + \varepsilon) \cos^q(\theta)\, G_c}\, AF^{(k)}(\varepsilon, \theta_{\mathrm{inc}}, \theta)\, \omega^{(k)} \right|^2}{N_0\, W} \tag{24}$$

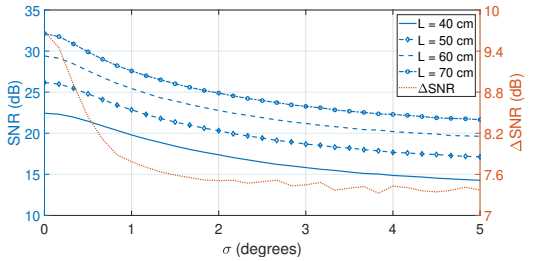

Fig. 4. SNR vs. σ and MS length L (left y-axis) and SNR difference between $L = 40$ and 70 cm (right y-axis) for $\tau = 12$, $q = 0.57$, $\theta_{\text{inc}} = 30°$.

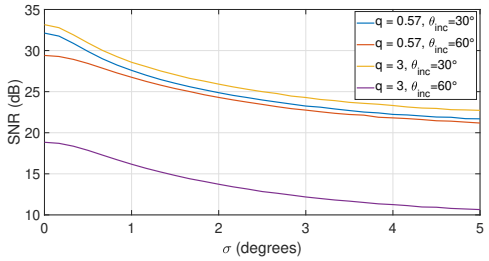

Fig. 5. SNR vs. σ for two values of q and θ_{inc} for $L = 70$ cm and $\tau = 12$.

$\sigma = 5°$. In summary we see that: 1) For a given σ, the SNR is higher for smaller HPBW, due to the beam higher gain; 2) For non-overlapping beams (dashed lines) the SNR degradation is stronger for smaller HPBW, as the beam is narrow; And 3) Higher beam gain results in slightly less sensitivity to BAE, provided that overlapping beams are used. Overall, for a given error magnitude, increasing the BS beam gain (by increasing the number of antenna elements) allows improving SNR.

VI. Conclusion

This paper studies the impact of beam misalignment in a wireless system employing a MS to improve coverage in a NLOS scenario. The MS is modeled by an array of small radiating unit cells each of them terminated with a complex load and beam misalignment is modeled using a truncated Gaussian distribution. In this context, an equivalent AF for the MS and an expression for the SNR experienced at the user in the presence of misalignment are derived. We show that beam misalignment can cause severe SNR degradation even in the presence of small errors. The numerical analysis reveals three important insights with practical implications from the system design point of view, namely: (1) The MS size and therefore the number of cells, can be used to compensate for the SNR degradation due to misalignment; (2) The use of low-gain unit cells can counteract the severe SNR degradation observed at larger angles of incidence; And (3) a higher BS beam gain can be used to compensate the SNR loss and to reduce the sensitivity against misalignment errors, provided that overlapping beams are used.

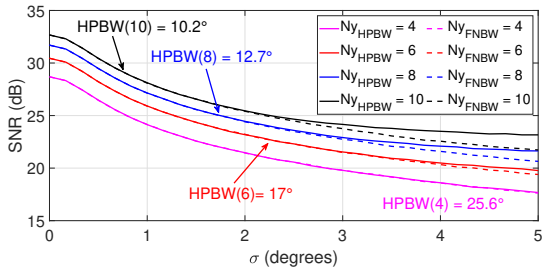

Fig. 6. SNR vs. σ for four values of HPBW for $L = 70$ cm and $\theta_{\text{inc}} = 30°$.

References

[1] Y. Li, A. Li, T. Cui, and D. F. Sievenpiper, "Multiwavelength Multiplexing Hologram Designed Using Impedance Metasurfaces," *IEEE Trans. on Antennas and Propagation*, vol. 66, no. 11, pp. 6408–6413, 2018.

[2] J. Hu, S. Bandyopadhyay, Y.-h. Liu, and L.-y. Shao, "A Review on Metasurface: From Principle to Smart Metadevices," *Frontiers in Physics*, vol. 8, 2021.

[3] E. Basar, "Transmission Through Large Intelligent Surfaces: A New Frontier in Wireless Communications," in *2019 European Conference on Networks and Comm. (EuCNC)*, 2019, pp. 112–117.

[4] Özdogan, E. Björnson, and E. G. Larsson, "Intelligent Reflecting Surfaces: Physics, Propagation, and Pathloss Modeling," *IEEE Wireless Comm. Letters*, vol. 9, no. 5, pp. 581–585, 2020.

[5] H. Li, R. Liu, M. Liy, Q. Liu, and X. Li, "IRS-Enhanced Wideband MU-MISO-OFDM Communication Systems," in *2020 IEEE Wireless Comm. and Networking Conference (WCNC)*, 2020, pp. 1–6.

[6] D. Dardari and D. Massari, "Using MetaPrisms for Performance Improvement in Wireless Communications," *IEEE Trans. on Wireless Comm.*, vol. 20, no. 5, pp. 3295–3307, 2021.

[7] M.-A. Badiu and J. P. Coon, "Communication Through a Large Reflecting Surface With Phase Errors," *IEEE Wireless Comm. Letters*, vol. 9, no. 2, pp. 184–188, 2020.

[8] N. Bahadori, N. Namvar, B. Kelleyy, and A. Homaifar, "Device-to-Device Communications in Millimeter Wave Band: Impact of Beam Alignment Error," in *2019 Wireless Telecomm. Symposium (WTS)*, 2019, pp. 1–6.

[9] Y. Quan, M. Coupechoux, and J.-M. Kélif, "Spatio-Temporal Wireless D2D Network With Imperfect Beam Alignment," in *2022 IEEE Wireless Comm. and Networking Conference (WCNC)*, 2022, pp. 2346–2351.

[10] W. Tang, M. Z. Chen, X. Chen, J. Y. Dai, Y. Han, M. Di Renzo, Y. Zeng, S. Jin, Q. Cheng, and T. J. Cui, "Wireless Communications With Reconfigurable Intelligent Surface: Path Loss Modeling and Experimental Measurement," *IEEE Trans. on Wireless Comm.*, vol. 20, no. 1, p. 421–439, Jan 2021.

[11] S. W. Ellingson, "Path Loss in Reconfigurable Intelligent Surface-Enabled Channels," in *2021 IEEE 32nd Annual Int. Symposium on Personal, Indoor and Mobile Radio Comm. (PIMRC)*, 2021, pp. 829–835.

[12] C. A. Balanis, *Antenna Theory Analysis and Design*. John Wiley & Sons, Inc., 2016.

[13] The Emergence of 5G mmWave. [Online]. Available: https://www.accton.com/Technology-Brief/the-emergence-of-5g-mmwave/

[14] G. Yang, J. Du, and M. Xiao, "Analysis on 60 GHz Wireless Communications with Beamwidth-Dependent Misalignment," *CoRR*, vol. abs/1611.07867, 2016. [Online]. Available: http://arxiv.org/abs/1611.07867

[15] F. Henschke, "Beamforming - How does it work," 2019. [Online]. Available: https://www.emf.ethz.ch

[16] S. Zhou, L. Chen, and W. Wang, "Attitude Information Aided mmWave Beam Tracking Based on Codebook," *IEEE Comm. Letters*, pp. 1–1, 2022.

[17] T. Cameron, "Bits to Beams – RF Technology Evolution for 5G mmwave Radios," in *EDI CON USA 2018*. [Online]. Available: https://www.edicononline.com/conference-papers-presentations/

[18] K. Kibaroglu, "28 GHz Phased-Array Transceivers for 5G Communications," Ph.D. dissertation, UC San Diego, 2018. [Online]. Available: https://escholarship.org/uc/item/5rd2245w